强激光与粒子束
High Power Laser and Particle Beams

利用八级铁校正衍射极限环中的失谐效应

宣守智　田顺强　刘新忠　龚奕豪　毛凌龙

Detuning effect corrections using octupoles in diffraction-limited storage ring

Xuan Shouzhi, Tian Shunqiang, Liu Xinzhong, Gong Yihao, Mao Linglong

引用本文:
宣守智, 田顺强, 刘新忠, 龚奕豪, 毛凌龙. 利用八级铁校正衍射极限环中的失谐效应[J]. 强激光与粒子束, 2025, 37: 074005. doi: 10.11884/HPLPB202537.240387
Xuan Shouzhi, Tian Shunqiang, Liu Xinzhong, Gong Yihao, Mao Linglong. Detuning effect corrections using octupoles in diffraction-limited storage ring[J]. *High Power Laser and Particle Beams*, 2025, 37: 074005. doi: 10.11884/HPLPB202537.240387

在线阅读 View online: https://doi.org/10.11884/HPLPB202537.240387

第 37 卷第 7 期
2025 年 7 月

强 激 光 与 粒 子 束
HIGH POWER LASER AND PARTICLE BEAMS

Vol. 37，No. 7
Jul.，2025

·Particle Beams and Accelerator Technology·

Detuning effect corrections using octupoles in diffraction-limited storage ring*

Xuan Shouzhi[1]， Tian Shunqiang[1,2]， Liu Xinzhong[1]， Gong Yihao[1]， Mao Linglong[2,3]

（1. *Shanghai Advanced Research Institute*, *Chinese Academy of Sciences*, *Shanghai* 201204, *China*;
2. *Shanghai Institute of Applied Physics*, *Chinese Academy of Sciences*, *Shanghai* 201800, *China*;
3. *University of Chinese Academy of Sciences*, *Beijing* 100049, *China*）

Abstract: The next generation of synchrotron radiation light sources features extremely low emittance, enabling the generation of synchrotron radiation with significantly higher brilliance, which facilitates the exploration of matter at smaller scales. However, the extremely low emittance results in stronger sextupole magnet strengths, leading to high natural chromaticity. This necessitates the use of sextupole magnets to correct the natural chromaticity. For the Shanghai Synchrotron Radiation Facility Upgrade (SSRF-U), a lattice was designed for the storage ring that can achieve an ultra-low natural emittance of 72.2 pm·rad at the beam energy of 3.5 GeV. However, the significant detuning effects, driven by high second-order resonant driving terms due to strong sextupoles, will degrade the performance of the facility. To resolve this issue, installation of octupoles in the SSRF-U storage ring has been planned. This paper presents the study results on configuration selection and optimization method for the octupoles. An optimal solution for the SSRF-U storage ring was obtained to effectively mitigate the amplitude-dependent tune shift and the second-order chromaticity, consequently leading to an increased dynamic aperture (DA), momentum acceptance (MA), and reduced sensitivity to magnetic field errors.

Key words: Shanghai Synchrotron Radiation Facility Upgrade, octupole, amplitude-dependent tune shift, dynamic aperture, momentum aperture

CLC number: TL54+4 **Document code:** A **doi**: 10.11884/HPLPB202537.240387

Next generation synchrotron radiation light sources[1-3] utilize multi-bend achromatic (MBA) lattices to significantly reduce beam emittance through strong focusing in storage ring. The necessarily strong sextupoles for chromaticity corrections generate highly irregular aberrations in particle motion that dramatically reduce dynamic aperture (DA) and momentum acceptance (MA)[4-5]. According to the perturbation theory in a dynamic system[6], this kind of aberration is decomposed into driving terms of different orders, comprehensively affecting the performance of the storage ring[7-8]. The higher-order driving terms independent of phase advance and the higher order chromaticity specifically induce tune shifts with oscillation amplitude and energy deviations, respectively, which we call detuning effects of the particle motion. Compared to the third-generation light sources that often adopt DBA and TBA lattices, MBA-based diffraction-limited storage rings exhibit more severe detuning effects. This makes is difficult for the particles with large oscillations or energy deviations to maintain the delicate cancellation of driving terms by setting linear phase advance between the sextupoles[9]. Control of the detuning effects has become a major challenge for weakening the sensitivity to magnetic field errors and optimizing DA and MA in diffraction-limited storage rings.

Octupoles are widely applied to increase detuning and thus enhance Landau damping in the storage rings of the light sources and the colliders[10-12]. However, in the diffraction-limited storage rings, the detuning effect induces a frequency shift of particles, causing them to approach the resonance line, which can result in particle loss. By reducing the detuning effect, the frequency shift of particles can be controlled, thereby improving the DA and MA[7]. The detuning has become so severe, which seriously affects the optimization of DA and MA. In this case, octupoles aim to reduce the detuning, which is different from the

* **Received date:** 2024-11-17; **Revised date:** 2025-06-11
Biography: Xuan Shouzhi, xuansz@sari.ac.cn。
Corresponding author: Tian Shunqiang, tiansq@sari.ac.cn。

previous applications[13]. The NSLS-II team presented a proposal for an octupole triplet to effectively control the detuning. Given that the variables to be controlled are three groups, the values of the octupole triplet in the calculated detuning term are fully determined. This part can be employed to increase the size of the DA. However, for MA, there are not too many terms to control. To control MA, additional grouped variables must be introduced. Their study results showed that both the DA and MA were sufficiently increased by adjusting the positions and strengths of two octupole triplets in the lattice[14].

A multi-objective optimization algorithm was applied in the nonlinear optimization, resulting in favorable outcomes for both DA and MA in the SSRF-U storage ring[15-17]. Particle Swarm Optimization (PSO)[18-19] is an evolutionary technique that simulates social behavior based on swarm intelligence. Due to its unique search mechanism, excellent convergence performance, and convenient computer implementation, PSO has found widespread applications in optimization. Multi-objective particle swarm optimization (MOPSO) algorithms have been applied to various optimization domains. In the design of the lattice for the next-generation synchrotron radiation source, efforts are directed towards minimizing the emittance while simultaneously ensuring that the DA remains within acceptable parameters. The application of optimization algorithms facilitates the generation of enhanced lattices, ensuring maximal reduction in emittance while preserving a satisfactory DA. We employ a MOPSO algorithm to optimize both the DA and MA.

For the Shanghai Synchrotron Radiation Facility Upgrade (SSRF-U) storage ring, a new space-saving scheme using an octupole quadruplet for control was proposed in this paper. The octupole quadruplet was symmetrically installed in the lattice. The octupole quadruplet comprises three octupoles for calculating the DA and an additional octupole for controlling the MA. This method introduces a novel variable that enables the control of the MA size relative to a group of octupole triplet forms, thereby reducing the space compared to the use of two groups of octupole triplet forms. The additional octuepoles enable the integration of theoretical calculations with optimization algorithms.

SSRF-U considers the influence of octupoles on DA and MA, and incorporates four octupoles inside to control DA and MA simultaneously. This scheme combines optimization algorithms with the theoretical design of octupoles. The aforementioned scheme does not necessitate the octupoles into straight sections, which impacts the efficiency of straight sections. It offers a basis for the enhancement of SSRF-U.

This paper introduces the design of the SSRF-U lattice and compares the effects before and after the addition of the octupole quadruplet. All tracking calculations were performed using the AT toolbox[20], lifetime calculations were performed using the elegant program[21].

1 Lattice design and nonlinear effect of the SSRF-U storage ring

The SSRF lattice was designed with twenty double-bend achromat (DBA) cells, organized into four super-periods. This layout encompassed sixteen 6.5-m-long straight sections and four 12-m-long straight sections, culminating in a circumference of 432 m. Two of the 12-m-long sections were designated for the injection system and the superconducting RF cavities' installation. The modification of the light source storage ring must maintain the existing layout, including the beamlines conforming to the current wall structure and aperture positions. The beamline layout should be kept as simple as possible, and this design should be retained for the SSRF-U.

1.1 Lattice design of the SSRF-U

The SSRF-U storage ring, designed for a beam energy of 3.5 GeV and with a natural emittance of 72.2 pm·rad, has successfully reached the diffraction limit for soft X-rays[22-23]. The beam optics and lattice layout for one super-period are shown in Fig.1. Each cell in the lattice, known as the 7BA cell, comprises seven dipoles, ten quadrupoles, and six sextupoles. The quadrupoles have a maximum gradient of 85 T/m, while the sextupoles have a maximum gradient of 5100 T/m^2. For chromaticity correction, six sextupoles are positioned on the high β and dispersion functions region. The

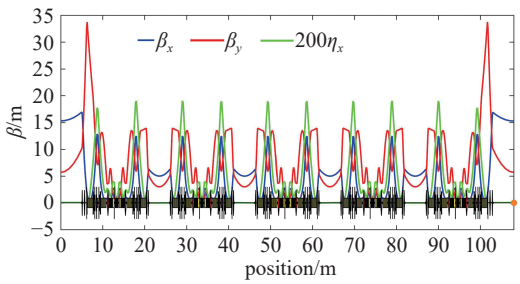

Fig. 1 Linear optical functions and magnet layout of the SSRF-U storage ring

raised horizontal beta functions at both ends are beneficial for increasing the DA. To further reduce the beam emittance of the lattice, the longitudinal gradient bend (LGB), in combination with anti-bend, is implemented. Similar structures can be observed in ESRF[24], HEPS[25], and APS-U[26].

The primary parameters of SSRF-U are summarized in Table 1. To avoid harmful nonlinear resonances, the betatron tunes for the new lattice were carefully chosen as 51.17 and 16.22 in the horizontal and vertical planes, respectively. The β functions were determined as follows: 15.29 m for the horizontal β function and 5.67 m for the vertical β function at the centers of long straight sections, and 5 m for the horizontal β function and 3 m for the vertical β function at the centers of standard straight sections. The natural chromaticity is −98.6/−68.1, but negative chromaticity may lead to strong head-tail instability. To mitigate this instability, sextupoles were used to correct the chromaticity to 3/3. However, the corrected chromaticity will lead to significant nonlinear effects, which are challenging for operation.

Table 1 Main parameters of the SSRF-U storage ring

energy/GeV	current/mA	circumference/m	tune	natural emittance/(pm·rad)	natural chromaticity	corrected chromaticity
3.5	500	432	51.17/16.22	72.2	−98.6/−68.1	3/3

1.2 Nonlinear effect of the SSRF-U

The design of SSRF-U combines nonlinear optimization with linear beam optics design, aiming to minimize emittance while maximizing DA. The MA only records the value at the injection point, and solutions outside the range of ±2% are considered invalid. However, the small DA remains a challenge for SSRF-U, as it hinders safe injection, and the low MA affects beam lifetime. The requirement for linear optics remains unchanged, therefore it will not be altered during the nonlinear optimization of SSRF-U.

The nonlinear effects in the SSRF-U can be analyzed through resonance driving terms (RDTs). These RDTs can be categorized into two types: geometric resonance driving terms and linear frequency shift terms.

Geometric resonance driving terms are phase-related and can be mitigated by adjusting the phase advance between the sextupoles. They generally induce resonances and reflect the strength of the resonant base. The geometric resonance driving terms can induce third-order resonances such as ν_x, $3\nu_x, \nu_x - 2\nu_y$, and $\nu_x + 2\nu_y$. These terms can lead to particle losses near these resonance lines. To minimize these effects, the phase advance between the sextupoles is usually considered to be adjusted to odd multiples of π. This ensures that the geometric terms of the sextupoles can cancel each other out.

The first-order geometric resonance driving term is phase-dependent. The first-order geometric resonance caused by sextupoles are calculated by Equation (1)[7].

$$\begin{cases} h(21000) = h^*(12000) = -\dfrac{1}{8}\sum_{i=1}^{N} b_{3i} L \beta_{xi}^{\frac{3}{2}} \mathrm{e}^{i\nu_{xi}} \\ h(30000) = h^*(03000) = -\dfrac{1}{24}\sum_{i=1}^{N} b_{3i} L \beta_{xi}^{\frac{3}{2}} \mathrm{e}^{i3\nu_{xi}} \\ h(10110) = h^*(01110) = -\dfrac{1}{4}\sum_{i=1}^{N} b_{3i} L \beta_{xi}^{\frac{1}{2}} \mathrm{e}^{i\nu_{xi}} \\ h(10020) = h^*(01200) = \dfrac{1}{8}\sum_{i=1}^{N} b_{3i} L \beta_{xi}^{\frac{1}{2}} \beta_{yi} \mathrm{e}^{i(\nu_{xi}-2\nu_{yi})} \\ h(10200) = h^*(01020) = \dfrac{1}{8}\sum_{i=1}^{N} b_{3i} L \beta_{xi}^{\frac{1}{2}} \beta_{yi} \mathrm{e}^{i(\nu_{xi}+3\nu_{yi})} \end{cases} \tag{1}$$

The FMAs were computed with tracking particles for 2000 turns. The diffusion rate was determined by analyzing the differences in frequencies calculated based on Fourier transformations of the data from the first 1 000 turns and the last 1 000 turns $\left(\nu_x^1, \nu_y^1\right) \to \left(\nu_x^2, \nu_y^2\right)$. Equation (2) represents the diffusion rate[27].

$$D = \lg \sqrt{\left(\nu_x^1 - \nu_x^2\right)^2 + \left(\nu_y^1 - \nu_y^2\right)^2} \tag{2}$$

The color bar in Fig.2 represents their diffusion rate, with red indicating a higher rate and therefore less stability, while blue indicating a lower rate and better stability. On the other hand, if the particle's motion is far from resonance, its

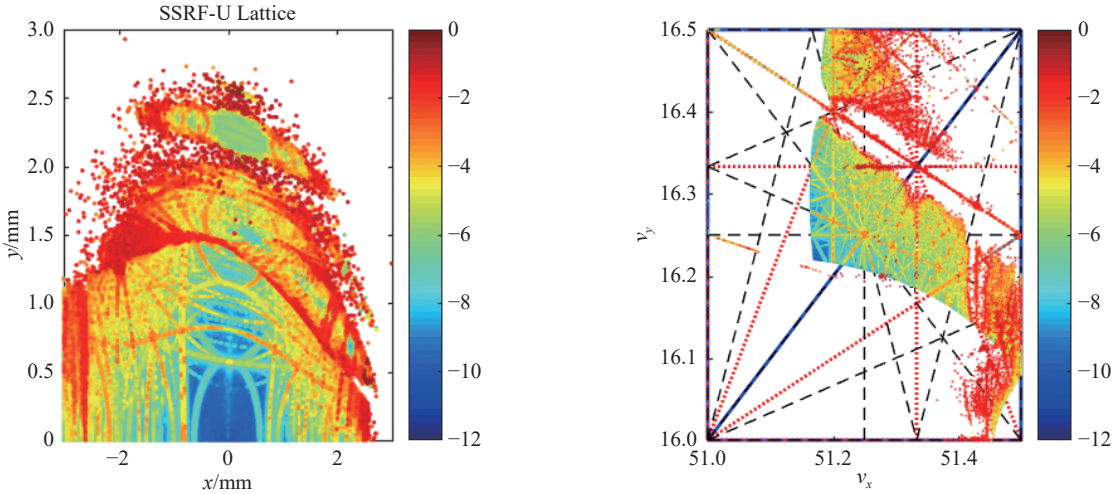

Fig. 2 Frequency map analysis (FMA) of SSRF-U

fundamental frequency vector can be accurately identified with minimal diffusion, indicating stable motion. If a particle's motion occurs within the random layer or on the resonance, its calculated frequency vector exhibits significant diffusion, indicating unstable motion.

The phase of sextupoles in SSRF-U is strategically positioned at near π and 3π, which effectively minimizes the geometric resonant driving terms. Table 2 provides a summary of the values for the linear geometric driving terms of SSRF-U. The DA and frequency maps (FMAs) are depicted in Fig.2, on-momentum DA (left) and, frequency footprint (right) in the long straight section of the SSRF-U storage ring. The red area in Fig.2 represents the detuned region where particles are more susceptible to magnetic errors, while the blue area represents the stable region. The DA without energy deviation exceeds ±2.0 mm in both the horizontal and vertical directions.

Table 2 Values of the geometric driving terms of SSRF-U

$h(21000)$	$h(30000)$	$h(10110)$	$h(10020)$	$h(10200)$
18.424 9+9.999 1i	3.421 4+46.619 7i	35.878 2+19.507 1i	123.11～105.61i	−0.274 6+2.610 0i

The FMA shows that particles will not be lost near the resonant lines corresponding to $3\nu_{x/y}$ the tunes for the SSRF-U have been selected with integer parts set to 51 for the horizontal tune and 16 for the vertical tune. Consequently, the ring closure of $\nu_x + 2\nu_y$ results in an overall tune of 84, which is a multiple of 4 due to the SSRF-U's four super-periods design. The particles captured in this line will experience resonance, and this factor dramatically increases the error sensitivity.

Although the tune of the SSRF-U has been carefully selected, the severe detuning causes large-amplitude particles oscillation frequency close to or across dangerous structural resonances. To mitigate the risks associated with these dangerous resonances, it is crucial to minimize the magnitude of tune shifts. Hence, the oscillation frequency can be kept as far as possible from these kinds of structural resonances. The tunes with amplitude can be expressed using Equation (3).

$$\begin{cases} \nu_x = \nu_{x0} + \dfrac{\partial \nu_x}{\partial J_x} J_x + \dfrac{\partial \nu_x}{\partial J_y} J_y + \text{higher-order} \\ \nu_y = \nu_{y0} + \dfrac{\partial \nu_y}{\partial J_x} J_x + \dfrac{\partial \nu_y}{\partial J_y} J_y + \text{higher-order} \end{cases} \tag{3}$$

The amplitude-dependent tune shift terms are represented by $\partial\nu_x/\partial J_x, \partial\nu_x/\partial J_y$, and $\partial\nu_y/\partial J_y$. For the SSRF-U, these three terms have values of $1.683\,4\times10^6$, $-1.030\,3\times10^5$, and $1.190\,6\times10^6$ respectively, falling within the range of 10^5 to 10^6. The higher-order effects become apparent with larger amplitudes, necessitating the use of octupoles to control these effects.

2 Application of octupoles to control tune shifts

The Hamiltonian for the thin octupole can be expanded with small momentum deviations and is expressed as follows

$$H = \frac{b}{4}\left(1+\delta+\delta^2\right)\left(x^4 - 6x^2y^2 + y^4\right) \tag{4}$$

The octupole Hamiltonian contains five phase-free terms, which can be expressed as equation[7]

$$\begin{cases} h_{22000} = \dfrac{3}{8} b\beta_x^2 J_x^2 \\ h_{11110} = -3b\beta_x\beta_y J_x J_y \\ h_{00220} = \dfrac{3}{8} b\beta_y^2 J_y^2 \\ h_{22001} = \dfrac{3}{2} b\beta_x J_x \eta^2 \delta^2 \\ h_{00112} = -\dfrac{3}{2} b\beta_y J_y \eta^2 \delta^2 \end{cases} \tag{5}$$

The J and $2\pi\nu$ are conjugate variables. The variation of tune can be expressed as

$$\Delta\nu = \frac{1}{2\pi}\frac{\partial H}{\partial J} \tag{6}$$

The first three terms of Equation (5), which express amplitude-dependent tune shift (ADTS). These can be calculated using the following formula[28]

$$\begin{cases} \dfrac{\partial \Delta\nu_x}{\partial J_x} = \dfrac{3}{8\pi} b\beta_x^2 \\ \dfrac{\partial \Delta\nu_y}{\partial J_y} = \dfrac{3}{8\pi} b\beta_y^2 \\ \dfrac{\partial \Delta\nu_x}{\partial J_y} = \dfrac{3}{4\pi} b\beta_x\beta_y \end{cases} \tag{7}$$

Equation (7) demonstrates that octupoles can be used to correct the ADTS and presents linear relationship between the strength of the octupoles and the ADTS. To correct the terms $\partial\nu_x/\partial J_x$, $\partial\nu_x/\partial J_y$, and $\partial\nu_y/\partial J_y$ by octupoles, the octupoles' strength can be computed by terms which are represented by β_x^2, $\beta_x\beta_y$, and β_y^2. Therefore, the octupole positions need to be carefully selected. The determination of the appropriate position can be carried out by calculating the octupole strength matrix as specified in Equation (8).

$$\boldsymbol{U} = \frac{1}{8\pi}\begin{bmatrix} \dfrac{1}{2}\beta_{x1}^2 & \dfrac{1}{2}\beta_{x2}^2 & \dfrac{1}{2}\beta_{x3}^2 \\ \dfrac{1}{2}\beta_{y1}^2 & \dfrac{1}{2}\beta_{y2}^2 & \dfrac{1}{2}\beta_{y3}^2 \\ \beta_{x1}\beta_{y1} & \beta_{x2}\beta_{y2} & \beta_{x3}\beta_{y3} \end{bmatrix} \tag{8}$$

The octupole strength matrix is calculated from the intensity matrix of the octupoles, based on the magnitudes of the ADTS in the bare lattice, represented by $\boldsymbol{\alpha} = [\partial\nu_x/\partial J_x; \partial\nu_x/\partial J_y; \partial\nu_y/\partial J_y]$. The octupole strength matrix, denoted as $\boldsymbol{K}$, can be calculated by Equation (9)[14].

$$\boldsymbol{K} = \boldsymbol{U}^{-1}\boldsymbol{\alpha} \tag{9}$$

Using octupole triplet enables effective correction of the three ADTS that are closely related to amplitude variations. The last two terms included in Equation (6), representing the second-order chromaticity terms and can be expressed as follows[7]

$$\xi_{x,y}^2 = \frac{1}{2}\frac{\partial^2 \nu_{x,y}}{\partial \delta^2} = \frac{1}{4\pi}\frac{\partial^2}{\partial \delta^2}\left(\frac{\partial H}{\partial J_{x,y}}\right) = \pm\frac{3b}{4\pi}\eta^2\beta_{x,y} \tag{10}$$

The second-order chromaticity terms are the consequence of the combined influence of quadrupoles and sextupoles in the dispersion region. These terms are reflected in the resonance driving terms h_{10002}, h_{20001}, and h_{00201}. The second-order chromaticity terms can cause a significant tune shift in relation to energy deviations. Consequently, the oscillation frequency of particles may approach linear and structural resonances, resulting in a reduction in the DA and MA.

Similarly, the second-order chromaticity terms are influenced by octupoles. Thus, the optimization of linear frequency shifts heavily relies on the positioning of octupoles placed in the dispersion region. The accurate placement and strength of octupoles directly change ADTS and MA. By carefully optimizing these factors, specifically the octupole positions and strengths, we can simultaneously enhance both the DA and MA.

3 Applications of octupoles in the SSRF-U storage ring

Due to the fact that the octupoles affects the fourth-order resonance term, the position of the octupoles affects DA and MA. The phase of the octupoles is usually an odd multiple of that of the sextupoles. However, simulations have shown that weakening these resonance-driven terms does not guarantee an increase in both the DA and MA. For this reason, a suitable location is required to ensure that weakened octupoles are produced to limit additional effects caused by the octupoles. The ratio of the octupoles can control the MA.

Two scenarios were considered to optimize the nonlinear effects of the SSRF-U: one involving an octupole triplet and the other involving octupole quadruplet. Equation (7) indicates that the optimal placement of the octupole triplet is near locations with high values of both β_x and β_y, as well as locations with same values of β_x and β_y. Octupoles are divided into three families, corresponding to *Oxx*, *Oyy*, *Oxy*, which control $\partial\nu_x/\partial J_x$, $\partial\nu_y/\partial J_y$ and $\partial\nu_x/\partial J_y$. Additionally, the octupole triplet should be placed closer to sextupole positions to mitigate second-order resonance driving terms.

In another scenario, an octupole quadruplet was used to improve the DA and MA. The positions of the octupoles in the quadruplet also had a significant impact. Two of the octupoles were initially set to fix the $\partial\nu_x/\partial J_y$, $\partial\nu_y/\partial J_y$ The correction octupole is $\partial\nu_y/\partial J_y$ divided into two parts. One corrects $\partial\nu_x/\partial J_x$ at lower dispersion, while the other is placed at larger dispersion to control MA. Thus the octupoles are divided into four families, *Oyy*1, *Oyy*2, *Oxy*, *Oxx*.

3.1 Optimizing the position and strength of octupoles using MOPSO algorithm

The strength of the octupoles needs to be taken into account. Equation (7) was utilized to calculate the strengths of three groups among the four octupoles. Due to the presence of higher-order terms, DA does not necessarily increase with full correction, so an additional variable on the setup ratio is needed.

Multi-Objective Particle Swarm Optimization (MOPSO) is an advanced evolutionary algorithm designed to address complex optimization problems involving multiple, often conflicting objectives. In MOPSO, each particle adjusts its position based on its own experience and the experience of neighboring particles, guided by mechanisms such as Pareto dominance, crowding distance, and external archives to maintain diversity and convergence toward the Pareto optimal front. The solutions to be found reside within the Pareto optimal front. MOPSO is particularly well-suited for solving multi-objective optimization problems.

Simulations have shown that the position of the octupole has a significant impact on both MA and DA in the case of octupole triplets. To achieve the desired values for DA and MA, MOPSO was employed. The variables for the octupole triplets are divided into four groups: the positions of the octupoles and the ratio of the theoretical values. In the case of octopole triplet the position needs to be at a larger β function in order to exert the greatest possible influence on the three ADTs and the values are calculated from the ADTS terms of the storage ring, which makes it challenging to simultaneously optimize DA and MA. It is clear that the triplet scheme is not satisfactory in the SSRF-U storage ring. This section does not display the relevant optimization results. The octupole quadruplets exhibits one additional octupole variable relative to the octupole triplet, which is not constrained by the theoretical values. Consequently, the position and strength of the octupole can be optimized through consideration of this variable. The variables for the octupole quadruplets are divided into six groups: the positions of the four octupoles, the value of the *Oxx*2 octupole family, and the ratio of the theoretical values of the other three octupodes. The objective functions are the DA and MA at the injection point.

The MOPSO algorithm aims to find a set of solutions that represent the Pareto front, providing a trade-off between conflicting objectives. Fine-tuning of parameters such as inertia weight (w), acceleration coefficients (c_1 and c_2) and the number of particles may be necessary to improve the performance of the algorithm. These parameters may need to be adjusted specifically for different problem domains.

Fig.3 shows the optimization results of MOPSO with 90 particles and 200 iterations. Fig.3(a) displays the overall distribution of particles across multiple generations, while Fig.3(b) presents the optimal results from the final generation. The selected octupoles are highlighted in green. In this context, DA refers to the area traced by particles over 1 000 turns, and EA represents the maximum acceptable energy deviation at the injection point during tracking. The left side of the figure displays the evolution of Pareto front of solutions, while the right side shows the final optimal solution set for the last generation. After

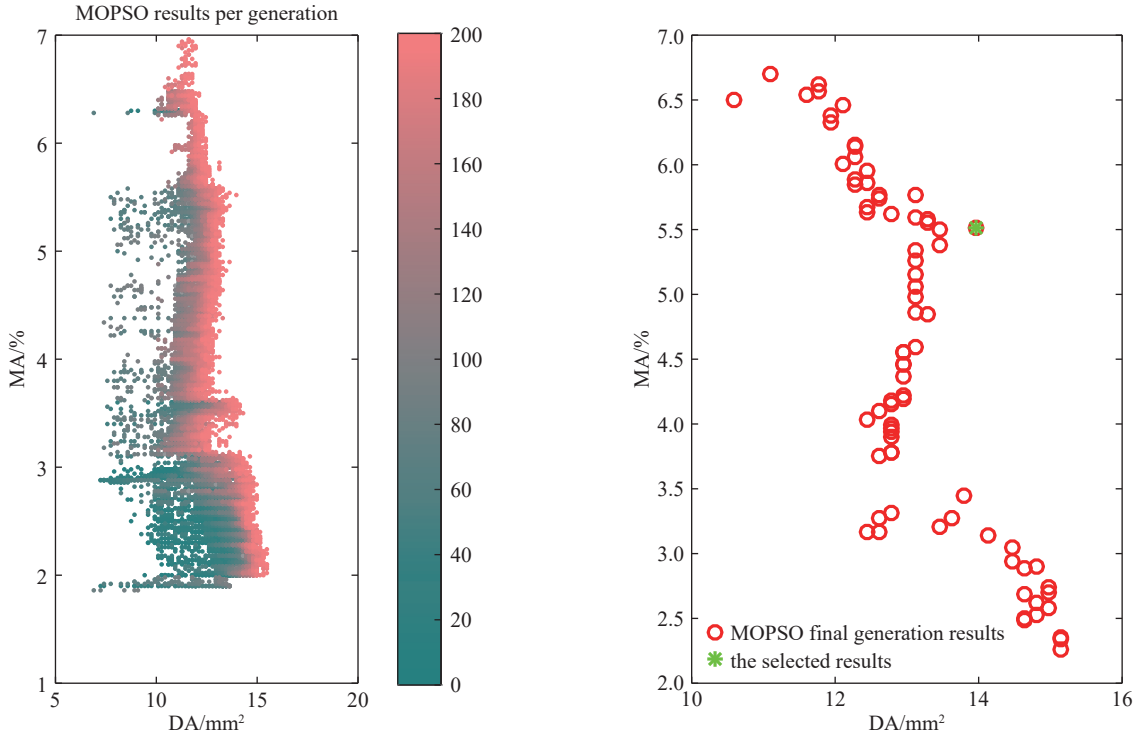

(a) the overall distribution of particles across multiple generations (b) the optimal results from the final generation

Fig. 3 The DAs and MAs of MOPSO optimization

optimization, the maximum integral strength of the octupoles is 5000 T/m^2 (the maximum gradient is 50000 T/m^3), which has no essential difficulty in magnet manufacture. The size of the DA increased from 8.9 mm^2 to 14 mm^2, and the MA increased from approximately 2.7% to 5.5%. The optimization process did not continue because of its sufficient effectiveness.

The positions of the octupole triplet and octupole quadruplets are shown in Fig.4 respectively. The upper section corresponds to the scenario with the octupole triplet, while the lower section depicts the configuration with the octupole quadruplet.

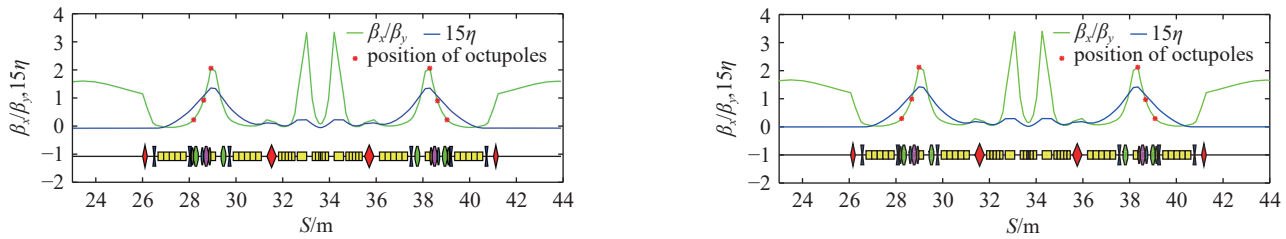

Fig. 4 The positions of the triple octupole and octupole quadruplet, as well as the values of β_x/β_y

Fig.4 shows the positions optimized by MOPSO. For three of the octupole positions, these solutions are close to the theoretical positions. At the same time, another octupole position with a lower β_x/β_y ratio position, corrects the $\partial\nu_y/J_y$. The octupoles are divided into four families, *Oyy*1, *Oyy*2, *Oxy*, and *Oxx*. The positions of *Oyy*1 and *Oyy*2 are in the lower and higher dispersions respectively. These octupoles together change to increase the MA.

3.2 Comparison of results using octupole triplet and octupole quadruplet in the SSRF-U

The FMA before and after the addition of octupoles are compared in Fig.5. The top part shows the FMA after adding the octupole triplet, and the bottom part shows the FMA after adding the octupole quadruplet. From Fig.5, it can be observed that the addition of the octupole triplet increases DA to 5 mm and significantly suppresses tune shift, preventing the tunes from the third-order resonance lines. When octupole quadruplets are added, the tune shift increases slightly, but the DA also increases to 5 mm. When only considering FMA, the addition of the octupole triplet is more effective. Further comparison is made by evaluating the MA in both cases.

Fig.6 presents the MA tracking results for three scenarios of the SSRF-U: without octupoles, with octupole triplet, and

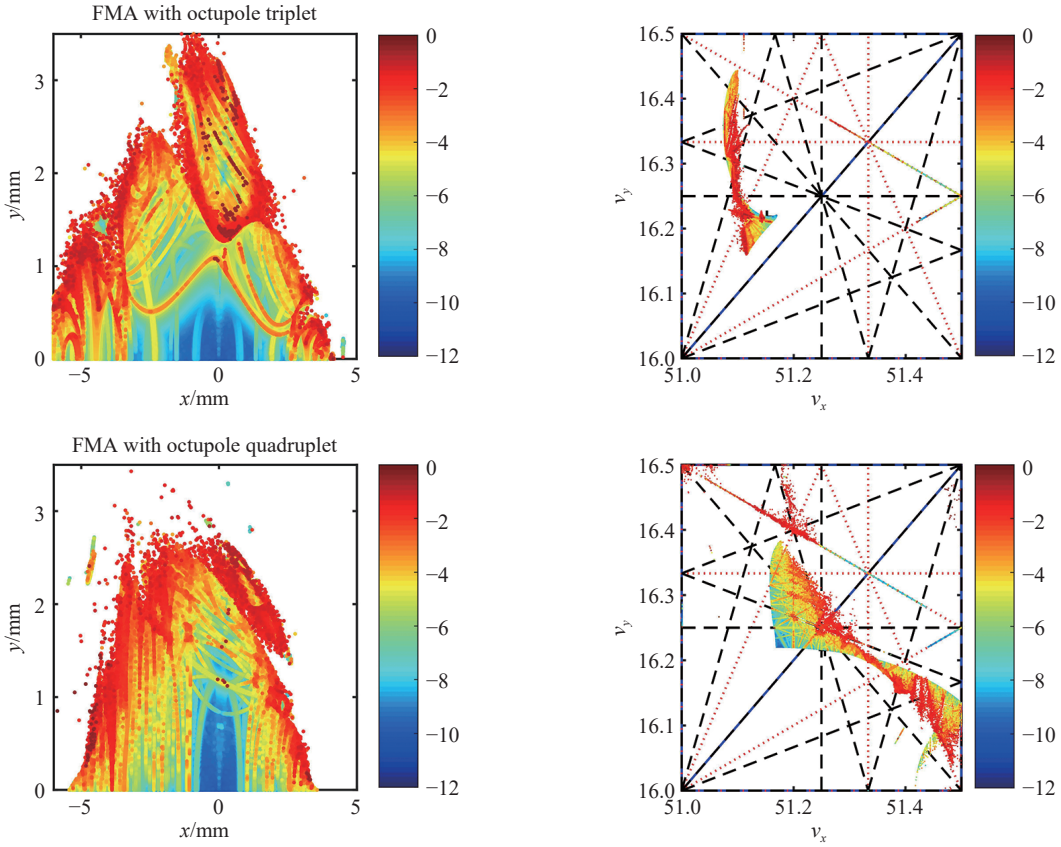

Fig. 5 The FMA after adding octupoles

with octupole quadruplet. The blue line represents the MA with the octupole triplet, the green line signifies the scenario without octupoles, and the red line indicates the values with the octupole quadruplet. The number of tracking turns was set to 2000, which is close to the 1/5 damping time.

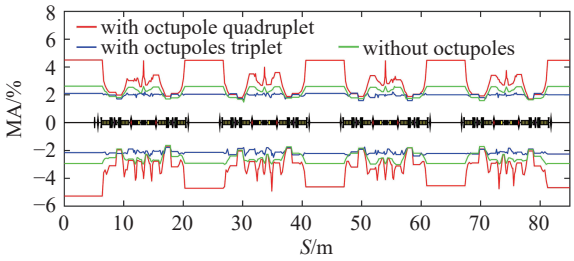

Fig. 6 The momentum acceptance of the SSRF-U in three cases

In Fig.6, the MA at the injection point in the bare lattices is approximately ±2.7%. However, when an octupole are is triplet is added, the MA decreases to 2%. After the addition of the octupole quadruplet, the MA at the injection point increases from 3% to about 5%. This enhancement in the MA at the injection point has a positive impact on the dynamic aperture (DA), especially for beams with energy deviations. The DAs for on-momentum and energy deviations of ±1.5% are shown in Fig.7.

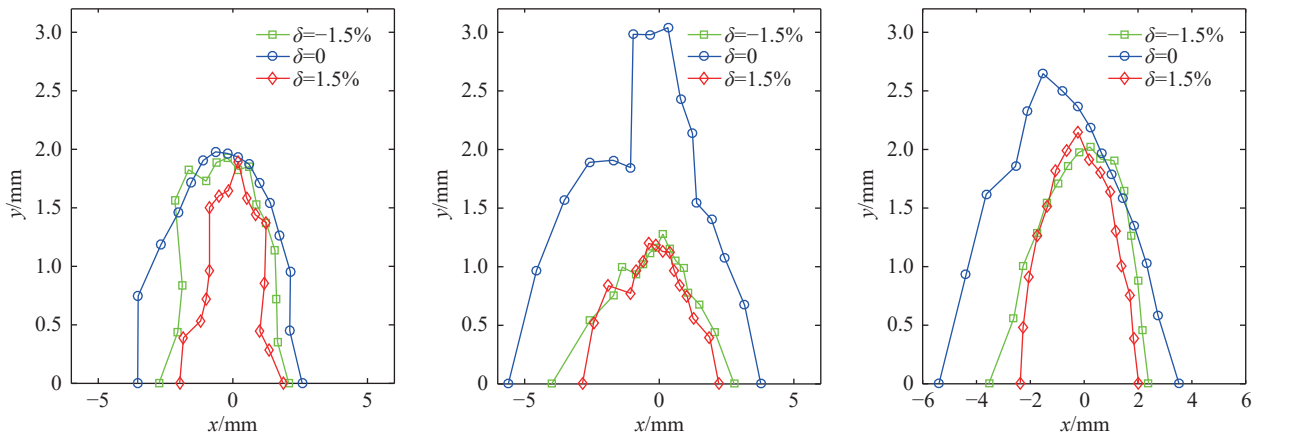

(a) dynamic aperture without octupoles (b) dynamic aperture with octupoles triplet (c) dynamic aperture with octupoles quadruplet

Fig. 7 The comparison between DA with and without octupoles

Fig.7 shows the DA of SSRF-U for on-momentum and energy deviations of ±1.5%. On the left side is the scenario without octupole magnets. In the middle is the situation with octupole triplet, and on the right side is the scenario with octupole quadruplet. Particle tracking for 2000 turns was performed.

From Fig.7, it can be observed the octupole triplet increases DA by about 60% compared to the bare lattice without energy deviation, while the DAs of octupole triplet are significantly reduced for the particles with energy deviations of ±1.5%. The DAs with octupole quadruplet are increased compared to both the bare lattice and the scenario with octupole triplet. The DAs with ±1.5% energy deviations increases to more than about three folds. The increased DAs and MAs contribute to an increase in Touschek lifetime.

Touschek lifetime is determined by the Twiss parameters, electron density, MA, and beam size. The equilibrium emittance, and bunch length, were computed using the IbsEmittance program[29].

The Touschek lifetime of the SSRF-U storage ring is shown in Fig.8. It can be observed that under the conditions of 500 MHz, 360 buckets, 500 mA, and 10% coupling, the beam lifetime in the lattice without octupole magnets is less than 1 h. However, the application of octupoles significantly extends the beam lifetime to nearly three hours, resulting in a threefold increase. Based on these comparisons, the best choice for SSRF-U storage ring would be the octupole quadruplet.

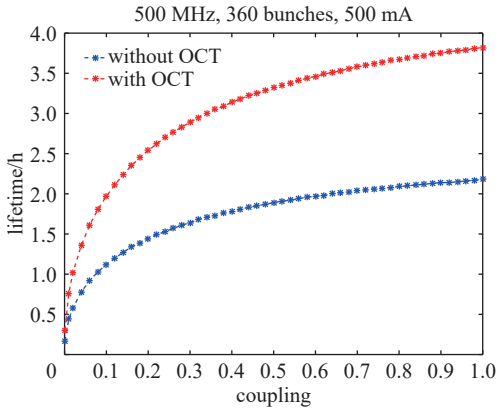

Fig. 8 The comparison between beam lifetime with and without octupoles

After examining both the octupole triplet and octupole quadruplet situations, it is more advantageous to choose the octupole quadruplet. This is because both the DA and MA directions are improved with this choice.

4 Error analysis after application of octupoles quadruplet

The magnet's random errors will have a significant impact on the DA and MA. The octupole quadruplet provides better control over the detuning effect, which should considerably improve the lattice's error resistance[30]. We compared the DA and MA with and without errors before and after applying the octupole quadruplet. Fig.9 illustrates the evaluations of the MA in one surper perriodicity of the SSRF-U storage ring with random magnetic errors up to the 10th order, which include normal and skew component both equal to 5×10^{-4}. The red lines represent the MA in ideal lattice, while the green lines represent the MAs with errors. For comparison, the ideal MA without octupole is also shown as black lines in Fig.9.

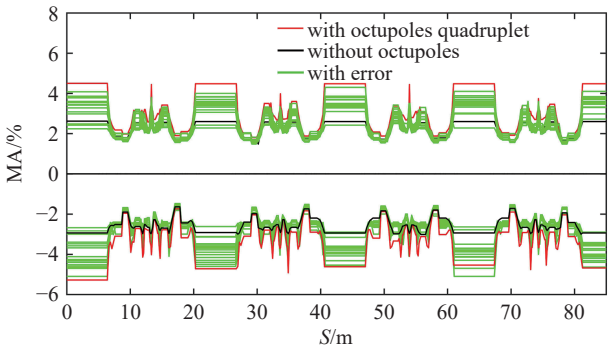

Fig. 9 The MA with 20 multipole error seeds of SSRF-U storage ring with octupoles

Fig.9 demonstrates that the addition of errors leads to a rapid decrease in the MA due to particles crossing severe resonances. However, in the injection section, the MA remains above 2% even in the presence of errors. The MAs are affected by magnetic errors but are mostly better than the case without octupoles.

Fig.10 depicts the DA of the SSRF-U under 50 sets of random errors in two scenarios: before and after application of octupole quadruplet. Particles were tracked using AT for 2000 turns. The red represents the DA at 1.5% energy deviation, green represents the DA at −1.5% energy deviation, and blue is the DA under normal conditions. Solid lines represent the scenario without errors, while dashed lines represent the scenario with errors from 50 sources.

Fig.10 shows that the DAs with 1.5% energy deviation are larger when using octupole quadruplets, compared to the DA without them. The DA is less affected by the error is due to theoretical calculation of octupole quadruplets by ADTS.

In Error analysis, octupole quadruplets is more advantageous than the octupole triplet for error perturbation. Additionally,

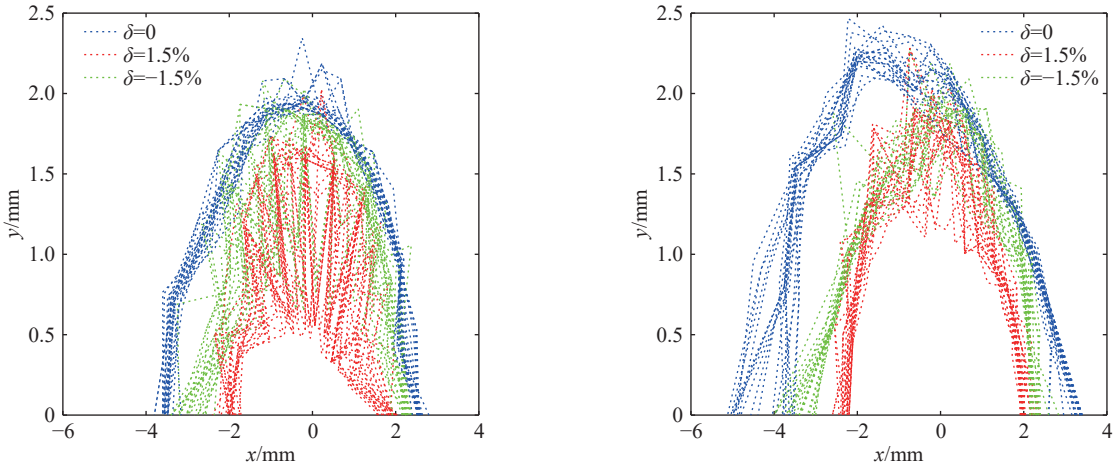

(a) DAs without octupoles (b) DAs with octupole quadruplet

Fig. 10 Dynamic acceptance with 20 multipole error seeds in three cases

octupole quadruplet can solve the problems in the SSRF-U storage ring caused by small DA and MA, and improve its performance.

5 Conclusion

This study compares the dynamics performances of both octupole triplet and octupole quadruplet schemes. The octupole quadruplet can effectively correct the ADTS term, resulting in an enhancement of DA and MA. The MOPSO algorithm was used to successfully optimize the DA and MA while controlling the strength of the octupole. Initially, the SSRF-U storage ring faced challenges with a low DA of 9.29 mm^2 and a MA of ±2.7%, impacting its injection efficiency and reducing its lifetime to under one hour. Octupole quadruplet schemes with the MOPSO algorithm, the DA increased by 46% to 13.58 mm^2, and the MA improved to ±5%, thereby significantly increasing the beam lifetime. Additionally, the optimized parameters showed enhanced resistance to errors, marking a substantial advancement in the stability of the SSRF-U. In order to save space in lattice, future research will consider using fewer magnets to optimise.

References:

[1] Tavares P F, Al-Dmour E, Andersson Å, et al. Commissioning and first-year operational results of the MAX IV 3 GeV ring[J]. Journal of Synchrotron Radiation, 2018, 25(5): 1291-1316.

[2] Jiao Yi, Xu Gang, Cui Xiaohao, et al. The HEPS project[J]. Journal of Synchrotron Radiation, 2018, 25(6): 1611-1618.

[3] Sun Yipeng, Borland M. Alternate lattice design for advanced photon source multi-bend achromat upgrade[C]//Proceedings of the 6th International Particle Accelerator Conference. 2015: 3-8.

[4] Tian Shunqiang, Hou Jie, Chen Guangling, et al. New chromaticity compensation approach and dynamic aperture increase in the SSRF storage ring[J]. Chinese Physics C, 2008, 32: 661664.

[5] Oide K, Koiso H. Dynamic aperture of electron storage rings with noninterleaved sextupoles[J]. Physical Review E, 1993, 47(3): 2010-2018.

[6] Chierchia L. Kolmogorov-Arnold-Moser (KAM) theory[M]//Meyers R A. Encyclopedia of Complexity and Systems Science. New York: Springer, 2009: 5064-5091.

[7] Bengtsson J. The sextupole scheme for the Swiss Light Source (SLS): an analytic approach[R]. Villigen: Paul Scherrer Institut (PSI), 1997: 97.

[8] Tian Shunqiang, Liu Guimin, Hou Jie, et al. Improved nonlinear optimization in the storage ring of the modern synchrotron radiation light source[J]. Chinese Physics C, 2009, 33(1): 65-73.

[9] Kim E S. Lattice design for a hybrid multi-bend achromat light source[J]. Nuclear Science and Techniques, 2020, 31: 68.

[10] Chattopadhyay S. Some fundamental aspects of fluctuations and coherence in charged-particle beams in storage rings[J]. AIP Conference Proceedings, 1985, 127(1): 467-623.

[11] Tambasco C, Pieloni T, Barranco J, et al. Beam transfer function measurements used to probe the transverse Landau damping at the LHC[J]. Physical Review Special Topics-Accelerators and Beams, 2020, 23: 071002.

[12] Gareyte J, Koutchouk J P, Ruggiero F. Landau damping dynamic aperture and octupole in LHC[R]. 1997.

[13] Plassard F, Hidaka Y, Li Yongjun, et al. Simultaneous compensation of phase and amplitude dependent geometrical resonances using octupoles[C]//Proceedings of the 12th International Particle Accelerator Conference. 2021.

[14] Plassard F, Wang Guimei, Shaftan T, et al. Simultaneous correction of high order geometrical driving terms with octupoles in synchrotron light sources[J].

Physical Review Special Topics-Accelerators and Beams, 2021, 24: 114801.

[15] Yang Lingyun, Robin D, Sannibale F, et al. Global optimization of an accelerator lattice using multiobjective genetic algorithms[J]. Nuclear Instruments and Methods in Physics Research Section A: Accelerators, Spectrometers, Detectors and Associated Equipment, 2009, 609(1): 50-57.

[16] Yang Lingyun, Li Yongjun, Guo Weiming, et al. Multiobjective optimization of dynamic aperture[J]. Physical Review Special Topics-Accelerators and Beams, 2011, 14: 054001.

[17] Tian Shunqiang. A design strategy of achievable linear optics for a complex storage ring lattice[J]. Chinese Physics C, 2010, 34(7): 1009-1015.

[18] Kennedy J, Eberhart R. Particle swarm optimization[C]//Proceedings of the ICNN'95-International Conference on Neural Networks. 1995: 1942-1948.

[19] Coello C A C, Pulido G T, Lechuga M S. Handling multiple objectives with particle swarm optimization[J]. IEEE Transactions on Evolutionary Computation, 2004, 8(3): 256-279.

[20] Terebilo A. Accelerator toolbox for MATLAB[R]. Menlo Park, CA, USA: SLAC National Accelerator Laboratory, 2001.

[21] Borland M. A flexible SDDS-compliant code for accelerator simulation[C]//Proceedings of the 6th International Computational Accelerator Physics Conference. 2000.

[22] Liu Xinzhong, Tian Shunqiang, Wu Xu, et al. Intra-beam scattering and beam lifetime in a candidate lattice of the soft X-ray diffraction-limited storage ring for the upgraded SSRF[J]. Nuclear Science and Techniques, 2021, 32: 83.

[23] Gong Yihao, Tian Shunqiang, Liu Xinzhong, et al. Highly coupled off-resonance lattice design in diffraction-limited light sources[J]. Nuclear Science and Techniques, 2024, 35: 163.

[24] Raimondi P, Carmignani N, Carver L R, et al. Commissioning of the hybrid multibend achromat lattice at the European Synchrotron Radiation Facility[J]. Physical Review Special Topics-Accelerators and Beams, 2021, 24: 110701.

[25] Jiao Yi, Duan Zhe, Guo Yuanyuan, et al. Progress in the design and related studies on the High Energy Photon Source[J]. Physics Procedia, 2016, 84: 40-46.

[26] Fornek T E. Advanced photon source upgrade project final design report[R]. Argonne, IL, USA, Argonne National Laboratory, 2019.

[27] Tian Shunqiang, Liu Guimin, Li Haohu, et al. Nonlinear optimization of the modern synchrotron radiation storage ring based on frequency map analysis[J]. Chinese Physics C, 2009, 33(2): 127-134.

[28] Leemann S C, Streun A. Perspectives for future light source lattices incorporating yet uncommon magnets[J]. Physical Review Special Topics-Accelerators and Beams, 2011, 14: 030701.

[29] Piwinski A. The touschek effect in strong focusing storage rings[DB/OL]. arXiv preprint arXiv: physics/9903034, 1999.

[30] Liu Xinzhong, Tian Shunqiang, Tan Liyuan, et al. Applications of vertical damping wigglers in an X-ray diffraction limited storage ring[J]. Nuclear Instruments and Methods in Physics Research Section A: Accelerators, Spectrometers, Detectors and Associated Equipment, 2023, 1056: 168653.

利用八级铁校正衍射极限环中的失谐效应

宣守智[1]， 田顺强[1,2]， 刘新忠[1]， 龚奕豪[1]， 毛凌龙[2,3]

（1. 中国科学院 上海高等研究院，上海 201204； 2. 中国科学院 上海应用物理研究所，上海 201800； 3. 中国科学院大学，北京 100049）

摘 要： 新一代光源具有极低发射度，产生更高亮度的同步辐射光，探索更小物质尺度。低发射度会使得四级铁强度提高，产生较高的自然色品，需要六极铁校正这些自然色品。为了达到衍射极限环要求，上海同步辐射光源升级改造（SSRF-U）设计新磁聚焦结构，低发射度设计，在 3.5 GeV 束流能量下实现了 72.2 pm·rad 的自然发射度。然而，由于高强度六极铁产生高度二阶共振驱动项会引起失谐效应，降低储存环性能。为了解决这个问题，计划在 SSRF-U 存储环中安装八极铁。介绍了八极铁选择和优化方法。得到了 SSRF-U 存储环的最优方案，可以有效地缓解振幅相关的调谐频移项和二阶色品，从而提高动力学孔径（DA）和动量接受度（MA），提高对磁场误差的容忍度。

关 键 词： 上海光源升级改造；八极铁；振幅相关频移项；动力学孔径；动量接受度